Am J Physiol Lung Cell Mol Physiol 308: L1274–L1285, 2015.
First published April 10, 2015; doi:10.1152/ajplung.00220.2014.

Influence of glutathione-*S*-transferase (GST) inhibition on lung epithelial cell injury: role of oxidative stress and metabolism

Marianne E. Fletcher,[1] Piers R. Boshier,[2] Kenji Wakabayashi,[1] Hector C. Keun,[3] Ryszard T. Smolenski,[4,9] Paul A. Kirkham,[5,6] Ian M. Adcock,[5] Paul J. Barton,[5] Masao Takata,[1] and Nandor Marczin[1,7,8]

[1]*Anaesthetics, Pain Medicine and Intensive Care, Imperial College London, London, United Kingdom;* [2]*Biosurgery and Surgical Technology, Imperial College London, London, United Kingdom;* [3]*Biomolecular Medicine, Department of Surgery and Cancer, Imperial College London, London, United Kingdom;* [4]*Department of Biochemistry, Medical University of Gdansk, Gdansk, Poland;* [5]*National Heart and Lung Institute, Imperial College London, London, United Kingdom;* [6]*Department of Biomedical Sciences, University of Wolverhampton, Wolverhampton, United Kingdom;* [7]*Department of Anaesthetics, Royal Brompton and Harefield NHS Foundation Trust, Harefield Hospital, Harefield, Middlesex, United Kingdom;* [8]*Department of Anaesthesia and Intensive Therapy, Semmelweis University, Budapest, Hungary;* [9]*Department of Surgery and Translational Medicine, University of Milano-Bicocca, Milano, Italy*

Submitted 11 August 2014; accepted in final form 1 April 2015

Fletcher ME, Boshier PR, Wakabayashi K, Keun HC, Smolenski RT, Kirkham PA, Adcock IM, Barton PJ, Takata M, Marczin N. Influence of glutathione-*S*-transferase (GST) inhibition on lung epithelial cell injury: role of oxidative stress and metabolism. *Am J Physiol Lung Cell Mol Physiol* 308: L1274–L1285, 2015. First published April 10, 2015; doi:10.1152/ajplung.00220.2014.—Oxidant-mediated tissue injury is key to the pathogenesis of acute lung injury. Glutathione-*S*-transferases (GSTs) are important detoxifying enzymes that catalyze the conjugation of glutathione with toxic oxidant compounds and are associated with acute and chronic inflammatory lung diseases. We hypothesized that attenuation of cellular GST enzymes would augment intracellular oxidative and metabolic stress and induce lung cell injury. Treatment of murine lung epithelial cells with GST inhibitors, ethacrynic acid (EA), and caffeic acid compromised lung epithelial cell viability in a concentration-dependent manner. These inhibitors also potentiated cell injury induced by hydrogen peroxide (H_2O_2), tert-butyl-hydroperoxide, and hypoxia and reoxygenation (HR). SiRNA-mediated attenuation of GST-π but not GST-μ expression reduced cell viability and significantly enhanced stress (H_2O_2/HR)-induced injury. GST inhibitors also induced intracellular oxidative stress (measured by dihydrorhodamine 123 and dichlorofluorescein fluorescence), caused alterations in overall intracellular redox status (as evidenced by NAD^+/NADH ratios), and increased protein carbonyl formation. Furthermore, the antioxidant *N*-acetylcysteine completely prevented EA-induced oxidative stress and cytotoxicity. Whereas EA had no effect on mitochondrial energetics, it significantly altered cellular metabolic profile. To explore the physiological impact of these cellular events, we used an ex vivo mouse-isolated perfused lung model. Supplementation of perfusate with EA markedly affected lung mechanics and significantly increased lung permeability. The results of our combined genetic, pharmacological, and metabolic studies on multiple platforms suggest the importance of GST enzymes, specifically GST-π, in the cellular and whole lung response to acute oxidative and metabolic stress. These may have important clinical implications.

N-acetylcysteine; ethacrynic acid; caffeic acid; reactive oxygen species; viability

ACUTE LUNG INJURY (ALI) and acute respiratory distress syndrome (ARDS) are life-threatening inflammatory disorders, which may result from both medical and surgical situations such as sepsis, heart surgery, and lung transplantation (41). Among these, ischemia and reperfusion injury constitutes a unique entity, wherein metabolic and oxygen starvation and subsequent reoxygenation can lead to the release and accumulation of reactive oxygen species (ROS) (4). ROS can directly oxidize and damage DNA, protein, and lipid membranes, inactivate antioxidant enzymes, and enhance expression of proinflammatory genes, ultimately leading to cell injury and apoptosis (11).

The glutathione-*S*-transferase (GST) antioxidant enzymes form a multifunctional superfamily of intracellular isozymes that catalyze the conjugation of reduced glutathione (GSH) with a variety of toxic compounds, including xenobiotics and oxidative intermediates (such as lipid and DNA hydroperoxides and aldehydes) (17, 18). This renders them less toxic and facilitates their removal from the cell (17, 18). Their key role in cellular detoxification protects macromolecules from attack by reactive electrophiles, such as ROS products, environmental carcinogens, and chemotherapeutic agents. Increasing evidence suggests that GST expression and function are important in both cancer progression (24, 39) and acute inflammatory conditions (23). For example, Luo et al. (23) demonstrated that treatment of mice with recombinant GSTP1 attenuated LPS-induced acute inflammation.

The clinical importance of diminished endogenous GST expression and activity is emerging. At least five of the eight GST genes in humans have functional polymorphisms where substitutions or deletions affect enzyme expression and activity and are present in up to 50% of the population (16). Such polymorphisms are believed to contribute to individual differences in the clearance of xenobiotics and oxidative stress products and to susceptibility to various inflammatory and proliferative pathologies (16). For instance, individuals with homozygous GSTM1 gene deletions appear to be more susceptible to DNA damage induced by GSTM1 substrates (32) and are more at risk of developing lung adenocarcinoma (7). Preliminary clinical studies also suggest that attenuated GST expression may contribute to ALI (25). Moradi and colleagues (25) showed that GSTM1 polymorphisms were associated with increased mortality in critically ill patients with ALI/ARDS. In the setting of lung transplantation, donor GST polymorphisms

Address for reprint requests and other correspondence: N. Marczin, Section of Anaesthetics, Pain Medicine and Intensive Care, Imperial College London, Harefield Hospital, Harefield, Middlesex, UK. (e-mail: n.marczin@imperial.ac.uk).

dramatically increased the development of primary graft dysfunction (8, 14). Despite these suggestions, the exact role of GST attenuation in lung cell injury, the basic mechanisms involved, and the relative impact of different GST isozymes are not known.

We hypothesized that GST attenuation would lead to increased intracellular oxidative stress affecting mitochondrial energetics and cellular metabolism, resulting in lung cell injury. To test these ideas, we studied the influence of pharmacological inhibitors ethacrynic acid (EA) and caffeic acid (CA) (1, 28, 29, 37, 49) and RNA silencing of GST isoforms on lung epithelial cell survival, ROS generation, and energetic/metabolic status in murine cell culture models of ALI. Finally, the physiological impact of GST inhibition was also explored using an ex vivo murine-isolated perfused lung (IPL) model by focusing on potential effects on lung mechanics and permeability.

MATERIALS AND METHODS

Cell culture. Murine lung epithelium (MLE)-12 cells (ATCC, Rockville, MD) were grown in Hanks medium (F12:MEM) supplemented with 1% penicillin/streptomycin and 5% fetal calf serum at 37°C in humid conditions with 5% CO_2-95% air. For hypoxia and reoxygenation (HR) experiments, we used deoxygenated culture medium (bubbled with 95% N_2-5% CO_2 gas mixture under sterile conditions) and a hypoxic chamber (Mini Galaxy A; Wolf Laboratories, York, UK). Cells were exposed to hypoxic conditions for 12 or 24 h. Subsequently, medium was exchanged for fresh, prewarmed, oxygenated medium, and cells were exposed to normoxic conditions for increasing periods of reoxygenation (2, 6, 12, or 24 h).

GST inhibition: method and efficacy. The pharmacological agents EA and CA were employed to attenuate activity of purified bovine liver GST (350 mU) or endogenous GSTs in cell lysates. The degree of inhibition was evaluated using the GST fluorometric activity assay kit (Biovision, Mountain View, CA). A linear increase in fluorescence at excitation/emission (ex/em) 380/460 nm was measured over the initial 10-min period and calculated as fluorescence U (FU)/min. A standard calibration curve was used to determine GST activity (mU) in unknown samples.

To complement the pharmacological data, we employed RNAi to specifically knockdown GST-μ or -π isoforms. This was achieved using predesigned GST-μ and -π ON-TARGETplus Smartpool siRNA (Dharmacon siRNA Technologies, Thermo Scientific, Glasgow, UK). In brief, 20 pmol of scrambled control or GST-targeting siRNA was introduced into MLE cells using Lipofectamine 2000 (Invitrogen, Carlsbad, CA). After 5 h, the siRNA-Lipofectamine medium was replaced with fresh medium, and cells were incubated for an additional 48 h before further experimentation.

The extent of siRNA-mediated knockdown of GST expression was evaluated by RT-PCR. Total RNA was extracted from transfected cells using the RNAeasy mini kit (Qiagen, Valencia, CA) (13) and quantified spectrophotometrically (Biophotometer Plus; Eppendorf, Stevenage, UK). Single-stranded cDNA was synthesized from 2 μg RNA with TaqMan RT-PCR reagents using GeneAmp PCR System 9700 (Applied Biosystems, Warrington, UK) (13). The cycling conditions were 25°C for 10 min, 48°C for 30 min, and 95°C for 5 min. cDNA was amplified using the TaqMan gene expression master mix (Applied Biosystems) and TaqMan probes specifically targeted against mouse GST-μ (Mm00833915_g1) and GST-π (Mm00496606_m1) (Applied Biosystems). A standard nucleic acid template and water were used as positive and negative controls, respectively. Variations in RNA loading between reactions were normalized by measurement of 18S ribosomal RNA (12). PCR was performed under recommended thermal-cycling conditions: initially 50°C for 2 min and 95°C for 10 min (for enzyme activation), followed by 40 cycles of 95°C for 15 s (cDNA denaturation) and 60°C for 1 min (probe annealing and extension). Data were collected using the ABI PRISM 7700 and Sequence Detection System 1.9.1 (Applied Biosystems) and analyzed using the comparative cycle threshold (Ct) method (5).

Protein expression was evaluated by Western blotting. In brief, protein extracts (50 μg) were separated on 10% SDS-PAGE, transferred to nitrocellulose membranes, and incubated overnight with polyclonal anti-GST-μ (1:500) or anti-GST-π (1:500) antibodies (Abcam, Cambridge, UK). Antibody binding was detected using peroxidase-conjugated anti-goat IgG (1:2,000; Cell Signaling Technology, New England Biolaboratories, Hitchin, UK) and chemiluminescence detection reagents (Amersham Biosciences, Little Chalfont, UK). Equivalent loading of protein samples was confirmed by mouse monoclonal anti-β-actin or anti-α-tubulin IgG (1:2,000; Sigma, St. Louis, MO).

Analysis of lung cell viability. The effect of GST inhibition on cell viability was evaluated under control conditions and in combination with known oxidative stress conditions: hydrogen peroxide (H_2O_2), tert-butyl hydroperoxide (tBH), or HR. Cell viability was analyzed by the 2,5-diphenyltetrazolium bromide (MTT) reduction assay (26). The optical density was measured as an index of cell viability, at 595 nm using an MRX II plate reader (Magellan Biosciences, Surrey, UK).

To delineate the involvement of apoptosis vs. necrosis, we employed the annexin V-FITC, propidium iodide (PI) apoptosis/necrosis detection kit (Sigma) and fluorescence-activated cell sorting (FACS)Calibur flow cytometer (Becton Dickinson, Franklin Lakes, NJ) (38). Harvested cells were exposed to annexin V-FITC and PI in binding buffer for 10 min in the dark at room temperature. Ten thousand events were acquired and analyzed using the CellQuest program. Cellular debris (with low forward- and side-light scatter) was excluded from the analysis. FITC and PI fluorescence were detected at 525 nm and 620 nm, respectively. Quadrant statistics display annexin V and PI fluorescence on the *x*- and *y*-axis, respectively, to identify viable cells (negative for both annexin V and PI), apoptotic cells (positive for annexin V, negative for PI), and late apoptotic dead cells (labeled with both annexin V and PI). In most instances, apoptosis involves activation of caspase cascades. To further evaluate the role of apoptosis, cells were treated in the presence or absence of 100 μM zVAD (Sigma), a broad-spectrum caspase inhibitor, and cell viability was assessed by MTT assay.

Detection of oxidative stress. The influence of GST inhibition on intracellular ROS was quantified using the ROS-sensitive fluorescent dyes dihydrorhodamine (DHR) and 2′,7′-dihydrodichloro-fluorescein diacetate (H_2DCF-DA) (Invitrogen). MLE cells were preincubated for 30 min with 5 μM DHR or 20 μM H_2DCF-DA before exposure to the GST inhibitor EA for 1 h. Cells incubated in media alone or H_2O_2 served as negative and positive controls, respectively. Following treatment, cells were harvested and resuspended in FACS wash buffer (PBS supplemented with 5 mM EDTA, 2% FCS, and 0.1% sodium azide). Samples were analyzed by flow cytometry at ex/em 495/525 nm. ROS quantification is reported as mean fluorescence intensity (MFI). To evaluate the role of specific ROS in EA-induced cytotoxicity, cells were preincubated for 1 h before EA treatment with the ROS scavengers, *N*-acetylcysteine (NAC, 10 mM) or cell permeable polyethylene glycol (PEG)-conjugated catalase (5,000 U/ml), or inhibitors of catalase (aminotriazole, ATZ, 10 mM), superoxide dismutase (diethyldithiocarbamate, DETC, 1 mM), NADPH oxidase (diphenyliodonium, DPI, 10 μM), and nitric oxide synthase (nitro-L-arginine methyl ester, L-NAME, 10 mM).

To evaluate the effect of GST inhibition on mitochondrial energetics (relative levels of ATP, ADP, and AMP) and redox status (reflected by NAD and NADH ratios) (2, 21, 31), intracellular adenine nucleotides were extracted from control and experimental cells as described previously (47) and measured by reverse-phase high-performance liquid chromatography (HPLC) and UV detection at 254

nm. Briefly, samples were extracted with ice-cold perchloric acid (0.4 M) and neutralized with equimolar KOH. $KClO_4$ was then precipitated by centrifugation, and the supernatant was retained. Levels of ATP, ADP, AMP, NAD^+, and ADPR, a breakdown product of NADH following acid precipitation (21, 31), were analyzed using the Agilent HPLC 1100 system. The mobile phase was 0.1 M potassium dihydrogen phosphate (pH 6.0) with 0.15 M potassium chloride as phase A and 15% acetonitrile in A as phase B with the Hypersil BDS column and a flow rate 0.9 ml/min. The concentration of each nucleotide was expressed as nanomoles per milliliter of extract with reference to external standards used for calculation of concentrations with reference to cell protein.

Protein carbonyls were estimated using a 2,4-dinitrophenylhydrazine (DNPH)-based procedure reported elsewhere (6, 33) with minor changes. Briefly, cell lysates containing 0.1 mg protein were incubated with 0.1% DNPH for 1 h at room temperature. Samples were precipitated by addition of 30% trichloroacetic acid. Following centrifugation, pellets were washed with ethanol:ethyl acetate (1:1 vol/vol) and dissolved in 8 M guanidine-hydrochloride, 13 mM EDTA, and 133 mM Tris pH 7.4. Optical density at 365 nm was determined using a Hitachi U-2000 UV-VIS spectrophotometer. The carbonyl content was calculated using Beer's Law and an extinction coefficient of 2.1×10^4 M/cm. Results are reported as nanomoles carbonyl per milligram of protein.

Metabonomics. Global metabolic changes associated with GST inhibition and oxidative stress were detected by metabonomic analysis (3). Cellular extracts from control and experimental groups were prepared for nuclear magnetic resonance (NMR) spectroscopy analysis. A Bruker DRX600 spectrometer (Bruker Biospin, Rheinstetten, Germany) was employed, operating at 600.13 MHz ^{1}H NMR frequency and 283 K. Raw spectra were phased, baseline corrected, calibrated to the trimethylsilylpropionic acid (TMSP) internal standard resonance ($d_H = 0.00$ ppm) and imported into Matlab (Student 2007; The MathWorks, Natick, MA). Spectra were normalized to protein. Isolated metabolite signals within spectra were defined through visual inspection, and their peak areas were determined. Metabolite assignment was made using the Madison Metabolomics Consortium Database (9).

Ex vivo IPL model. To investigate the physiological relevance of our cellular findings, the direct impact of GST inhibitor EA on lung physiological parameters was explored using an IPL mouse model. All procedures were approved by the United Kingdom Home Office in accordance with the Animals (Scientific Procedures) Act 1986, UK. Male C57BL6 mice (Charles River Laboratories, Margate, UK) aged 8–12 wk were used for the ex vivo IPL system (Hugo Sachs Elektronik; Harvard Apparatus, March-Hugstetten, Germany). In brief, mice were anaesthetized, tracheostomized, and ventilated with a custom-made mouse ventilator as previously described (35) at a respiratory rate of 80 breaths/min. After thoracotomy/laparotomy and heparinization, animals were exsanguinated, and the pulmonary artery and left atrium were cannulated. Lungs were perfused in a nonrecirculating manner with prewarmed RPMI 1640 supplemented with 4% BSA and 1.4 g/l NaCl (Sigma) to increase osmolarity, as described previously (34). All experiments had an initial 15-min equilibration period, and low tidal volume (VT) of 8 ml/kg was applied throughout to minimize lung injury development. Peak inspiratory pressure (PIP), positive end-expiratory pressure, and gas flow were monitored continually via transducers connected to a PowerLab data acquisition system (AD Instruments, Chalgrove, UK). Data were analyzed using Chart software (version 5.5.6, AD Instruments). Accurate measurements of VT, respiratory system compliance, and resistance were determined by end-inflation occlusion at 30-min intervals.

Lung permeability index. The pulmonary endothelial/epithelial permeability to a fluorescence-labeled albumin was assessed, using an adaptation of a previously reported fluorescence-based method for measuring vascular leak into the alveolar space (45). Following a 2-h perfusion, 1 mg/ml Alexa Fluor 594-conjugated albumin (Invitrogen) was added to the perfusate in the recirculating circuit. After 30 min, the perfusate was collected from the reservoir and stored in the dark. Thereafter, the circuit was switched to a nonrecirculating system for 5 min to wash out the residual fluorescence from the lung vasculature. Bronchoalveolar lavage fluid (BALF) was obtained as described previously (44). Fluorescence levels of perfusate, BALF, and lung tissue were measured using a fluorescence plate reader (Flx-800; BioTek Instruments, Potton, UK) at absorption 590 nm. An index of lung endothelial and epithelial permeability was then estimated by the ratio of lung tissue:perfusate and lavage fluid:perfusate fluorescent signal, respectively. Protein levels in BALF were also quantified as another index of pulmonary permeability.

Statistics. Data are reported as the means of repeated experiments ± SD. The majority of statistical analyses were performed using Prism software (version 4.0; GraphPad, La Jolla, CA). Metabonomics data were analyzed by SPSS 17 (Chicago, IL). Comparison of three or more variables was carried out by either one-way ANOVA or repeated-measure ANOVA with multicomparisons/post hoc tests (including Bonferroni) where appropriate. Statistical significance of metabonomics data was assessed by Kruskal-Wallis test. Multiple comparisons of metabonomics data were controlled for using the Benjamini-Hochberg procedure, with accepted false discovery rate 0.05. A P value <0.05 was considered significant.

RESULTS

EA and CA inhibit GST activity and decrease lung cell viability. To study the efficiency of GST inhibition, pure GST and MLE cell lysates (prepared from 4×10^6 cells) were incubated with increasing concentrations of GST inhibitors at 37°C for 1 h. Both EA and CA effectively inhibited GST activity in pure GST as well as MLE cell lysates in a concentration-dependent manner with an IC_{50} of ~25 μM and 1 mM, respectively. Exposure of MLE cells to increasing concentrations of EA and CA revealed major morphological changes and a concentration-dependent reduction in cell viability, assessed by MTT assay. After 5-h exposure, 100 and 300 μM EA reduced viability to 92 ± 7% and 13 ± 7% of control (Fig. 1*A*).

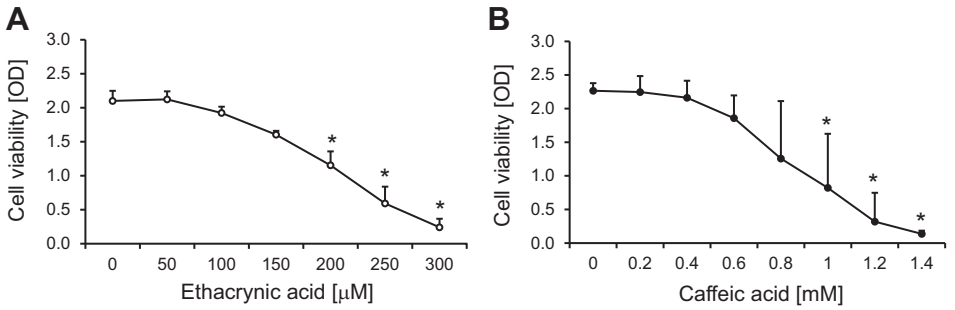

Fig. 1. Influence of increasing concentrations of glutathione-*S*-transferase (GST) inhibitors on murine lung epithelium (MLE) cell viability. Viability was assessed by 2,5-diphenyltetrazolium bromide (MTT) assay following 5-h ethacrynic acid (EA) exposure (*A*) and 24-h treatment with caffeic acid (CA) (*B*); $n = 4–6$; *$P < 0.05$ vs. untreated control.

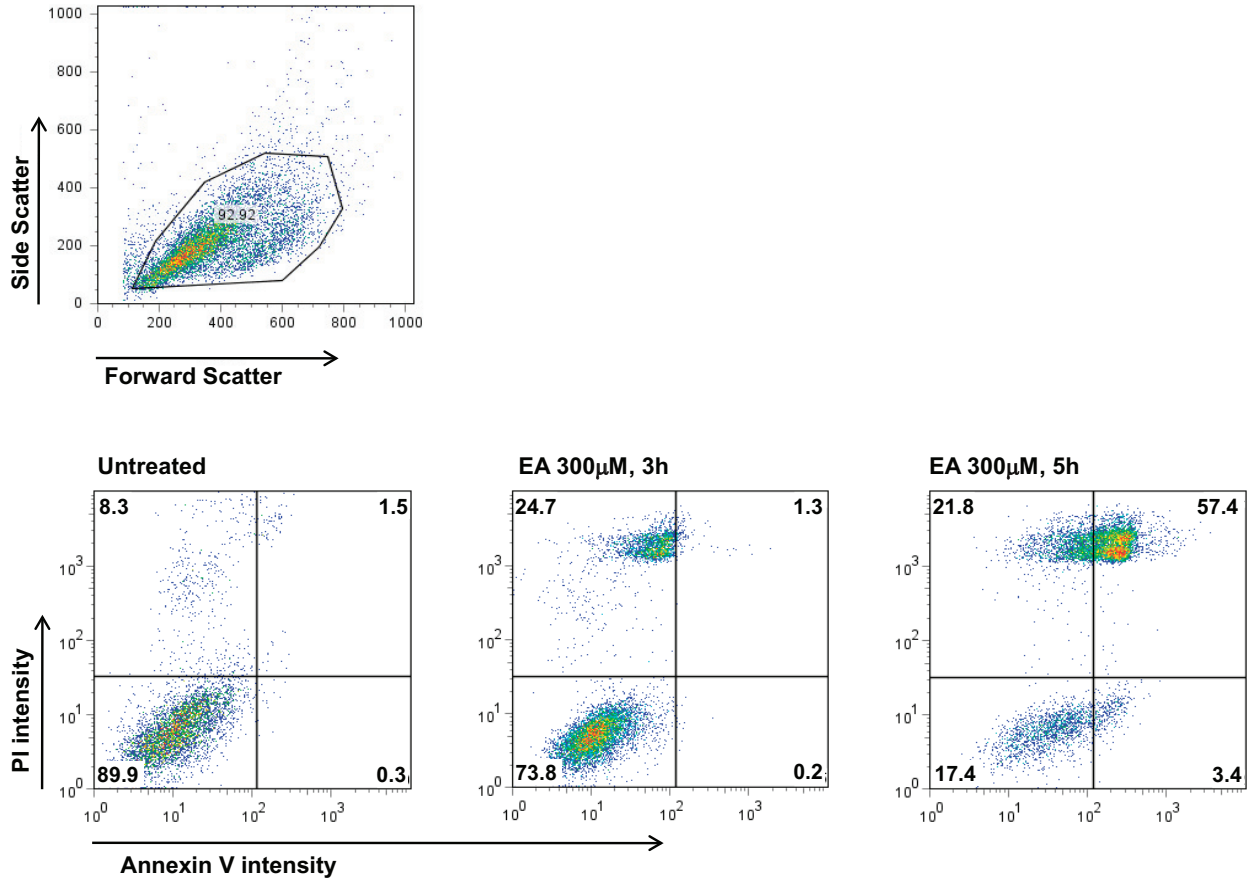

Fig. 2. Apoptotic/necrotic cells determined by annexin V (Ann V)/propidium iodide (PI) staining and flow cytometry. Cells were treated with 300 μM EA for the indicated times, and untreated cells were used as a negative control. A representative forward-scatter/side-scatter gating strategy is illustrated to exclude cell debris from the analysis. The gated cell population was then acquired for Ann V and PI staining. Viable: Ann V and PI negative. Apoptotic: Ann V positive and PI negative. Necrotic: PI positive. Apoptotic/Necrotic: Ann V and PI positive.

Similar findings were obtained following 24-h treatment with CA, which led to a 55 ± 35% reduction in cell viability at 1 mM (Fig. 1*B*). To explore whether GST inhibitor-induced cytotoxicity was limited to epithelial cells or applicable to other cell types in the lung, we have explored the effect of EA on primary mouse lung endothelial cells available in our laboratory. Exposure of these cells to increasing concentrations of EA for 5 h showed that the endothelial cell viability was also compromised by 300 μM EA (74 ± 7% of control).

Apoptotic nature of cell death. The nature of EA-induced cell death was investigated by staining MLE cells with annexin V and PI, and fluorescently labeled cells were identified using FACS (Fig. 2). Untreated cells showed 90% cell viability, which decreased to 74% and 17% following 3- and 5-h incubation with 300 μM EA, respectively. This was associated with a significant rise in the necrotic cell population, i.e., those exhibiting PI fluorescence in the absence of annexin V labeling. Moreover, after 5 h of treatment, the percentage of annexin V-fluorescent cells increased by >10-fold, indicative of an apoptotic cell population. Cells exhibiting both annexin V and PI increased from 1 to 57% of total population.

To identify whether caspases are involved in EA-induced cell injury, MLE cells were incubated with zVAD (100 μM) before treatment with 0–300 μM EA (Fig. 3*A*). As a positive control, we evaluated whether zVAD preincubation influenced cell death induced by a combination of tumor necrosis factor-α

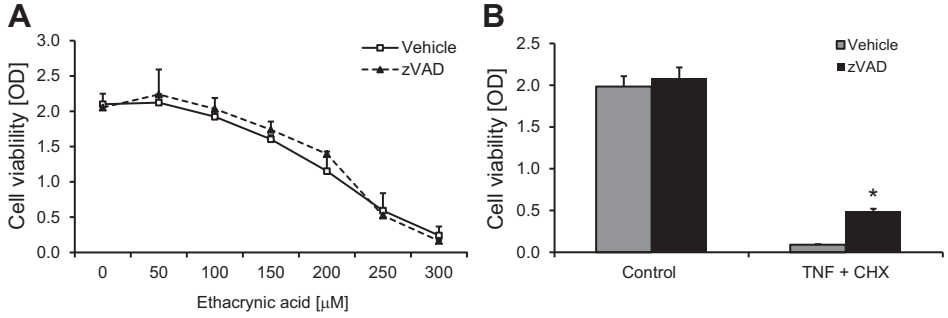

Fig. 3. Influence of caspase inhibitor zVAD on stress-induced MLE cell death. MLE cells were exposed to stresses EA (*A*) and tumor necrosis factor-α (TNF-α)/cycloheximide (CHX) (*B*) for 5 and 24 h, respectively; $n = 3–6$; *$P <$ 0.05 vs. vehicle control (i.e., in the absence of zVAD).

(TNF-α)/cycloheximide treatment (Fig. 3*B*). Whereas zVAD preincubation attenuated cell death induced by TNF/cycloheximide (cell viability of 24% vs. 5%), it had no influence on EA-induced cell death.

Potentiation of stress-induced cytotoxicity by GST inhibitors. H_2O_2 and tBH alone resulted in a concentration-dependent reduction in cell viability over 5 h. These stress-induced cytotoxic effects were significantly potentiated by subtoxic concentrations of GST inhibitors, namely 100 μM EA (Fig. 4, *A* and *C*) and 0.5 mM CA (Fig. 4*B*). For instance, cell viability was reduced from 64 ± 24% after 0.5 mM H_2O_2 treatment to 26 ± 14% and 31 ± 5% in the presence of EA and CA, respectively, compared with untreated controls. Similarly, EA exacerbated tBH-induced cell death. For instance, following 1 mM tBH treatment, the presence of GST inhibitor reduced viability from 71 ± 4% to 23 ± 14% of untreated controls.

Before studying the influence of EA on MLE cell survival in the setting of HR, we explored the influence of increasing duration of HR on cell viability. Interestingly, hypoxia up to 24 h and reoxygenation up to 6 h did not appear to compromise MLE cell viability measured as MTT activity (Fig. 4*D*). Injury, however, was unmasked in the presence of EA. For instance, 25 μM EA had no measurable effect during normoxia, but it reduced viability of hypoxic control by 19 ± 9%. In addition, 50 μM EA reduced cell viability by 35 ± 11% in normoxic conditions but led to a 77 ± 10% decrease in viability during HR conditions.

Oxidative stress is involved in EA-induced cytotoxicity. To test the hypothesis that EA-induced cell injury is mediated by an altered intracellular redox state (1, 37), we initially monitored oxidative stress with redox-sensitive fluorescent dyes. Exposure of MLE cells to EA (300 μM) for 1 h increased the MFI of DHR123 and DCF by over 2- and 30-fold, respectively, compared with basal levels (Fig. 5, *A* and *B*). In the control experiment, EA had no direct effect on dye autofluorescence in the absence of MLE cells after 3 h (data not shown).

To assess global intracellular redox state, nucleotides NAD^+ and ADPR (the breakdown product of NADH) were measured by HPLC and UV detection, and their ratio was calculated. Figure 5*C* shows that redox state was altered in a concentration-dependent manner by EA exposure alone, causing a decrease in NAD^+/NADH ratios to 11% of untreated control by 300 μM EA. Furthermore, H_2O_2 also reduced NAD^+/NADH ratios, and this effect was potentiated by EA (43 vs. 28% of untreated control following 3-h treatment with H_2O_2 in the absence or presence of 100 μM EA, respectively, $P < 0.05$) (Fig. 5*D*).

To further evaluate intracellular oxidative stress in the setting of GST inhibition, excess formation of carbonylated protein was monitored spectrophotometrically. Exposure of cells to 100 μM EA alone did not affect steady-state levels of protein carbonylation (Fig. 5*E*). H_2O_2 alone increased protein carbonyls from 1.2 ± 0.2 to 2.6 ± 0.3 nmol/mg, and EA significantly enhanced H_2O_2-induced increase in protein carbonyls from two- to fourfold, compared with untreated control after 3 h of treatment (Fig. 5*E*).

Inhibitors of H_2O_2 and NO do not attenuate EA-induced cell injury. We have attempted to further characterize the reactive species involved in EA-mediated lung cell injury. Specifically, to test the hypothesis that increased generation of H_2O_2 is responsible for EA-induced cell injury (37), we investigated the effect of modulating catalase activity by preincubating cells with either cell-permeable (PEG-conjugated) catalase (5,000 U/ml) or the catalase inhibitor ATZ (20 mM). Although catalase completely abolished the cytotoxic effect of H_2O_2 (Fig. 6*B*), EA-induced cell injury was unaffected by PEG catalase (Fig. 6*A*). ATZ-induced catalase inhibition also had no influence on EA cytotoxicity (Fig. 6*C*).

To further evaluate the role of intracellular oxidative stress in GST inhibitor-induced cytotoxicity, we preincubated cells with a variety of inhibitors, affecting well-known oxidative stress pathways and the broad-spectrum antioxidant NAC. Exposure of cells to L-NAME and DPI, targeting ROS gener-

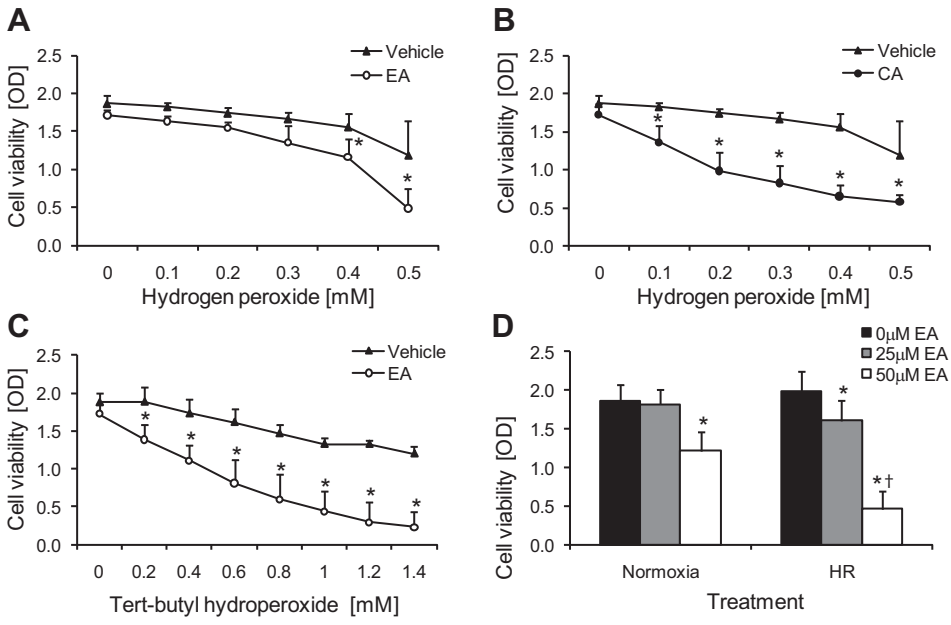

Fig. 4. Impact of GST inhibition on MLE cell response to oxidative stress conditions. Influence of chemical stressors hydrogen peroxide (H_2O_2) (*A* and *B*) and tert-butyl hydroperoxide (tBH) (*C*) on cell viability, determined by MTT assay, in the absence (▲) and presence of GST inhibitors EA (○) and CA (●). *D*: exposure of cells to 24 h of either normoxic or hypoxia (24 h) followed by reoxygenation (6 h) (hypoxia/reoxygenation, HR) in the presence of indicated concentrations of EA; $n = 5$; *$P < 0.05$ vs. vehicle controls (without GST inhibitors); †$P < 0.05$ vs. appropriate normoxic control.

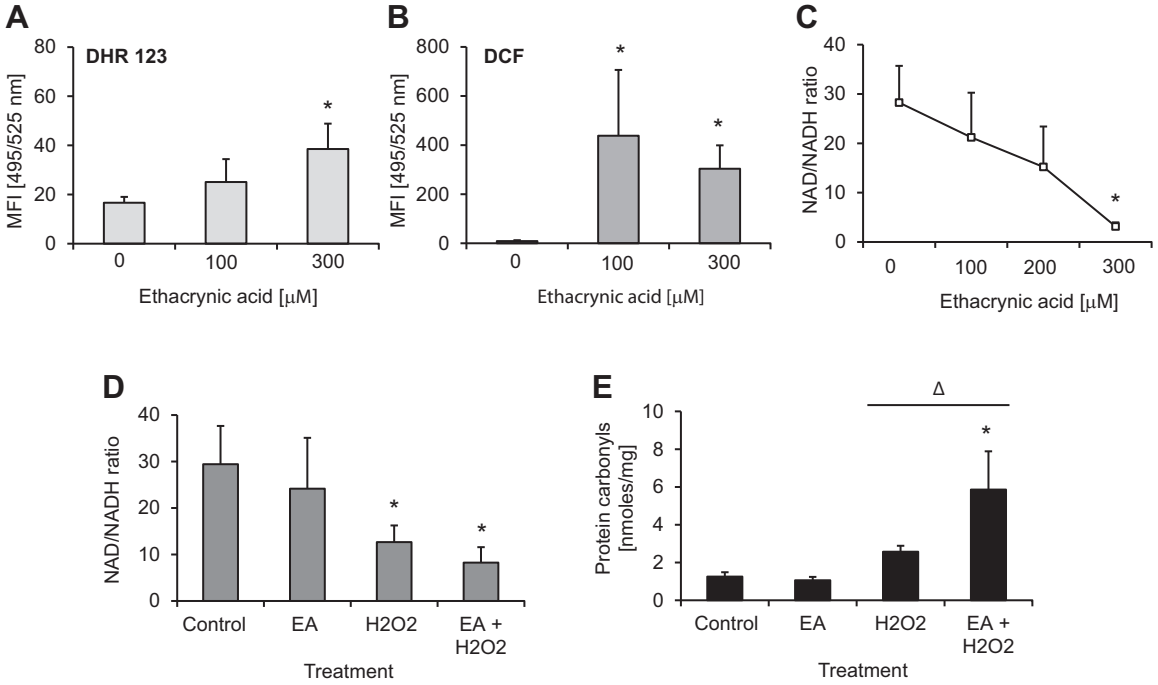

Fig. 5. Influence of GST inhibitor EA on intracellular oxidative stress measured by fluorescence of redox-sensitive dyes dihydrorhodamine 123 (DHR123) (*A*) and dichlorofluorescein (DCF) (*B*) fluorescence, following 1-h incubation with indicated concentrations of EA; $n = 5$. MFI, mean fluorescence intensity. Intracellular redox status was assessed by NAD^+/NADH (by measuring ADPR, a breakdown product of NADH under acid precipitation conditions) ratio following increasing concentrations of EA (over 1 h) (*C*) and EA (100 μM) treatment (*D*) with or without 0.8 mM H_2O_2 stress over 3 h; $n = 3$. *E*: influence of EA (100 μM) and/or H_2O_2 (0.8 mM) on protein carbonyl levels after 3-h treatment; $n = 3$; $^*P < 0.05$ vs. untreated control, $\triangle P < 0.05$ vs. cells exposed to H_2O_2.

ators nitric oxide synthase and NADPH oxidase, respectively, had no impact on EA-induced cell death. However, cells preincubated with the ROS scavenger NAC (10 mM) fully protected cells from injury induced by 300 μM EA (92 ± 6% vs. 13 ± 7% of untreated control, $P < 0.05$) (Fig. 7*C*) and 1 mM CA (84 ± 6% vs. 45 ± 35% of untreated control, $P < 0.05$) (Fig. 7*D*). Furthermore, pretreatment with NAC completely abolished EA-induced increased fluorescence (MFI) of ROS-sensitive dyes DHR123 and DCF (45 ± 8% vs. 14 ± 2% and 352 ± 49% vs. 9 ± 1%, $P < 0.05$) (Fig. 7, *A* and *B*).

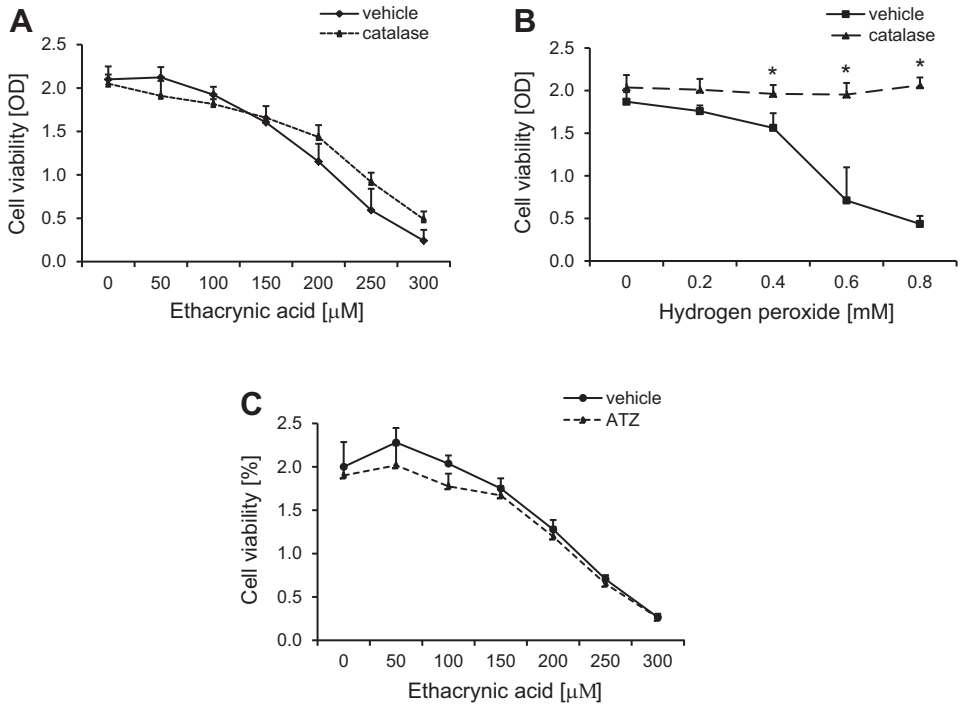

Fig. 6. Influence of catalase on EA-induced (*A*) and H_2O_2-induced (*B*) MLE cell death. Cells were treated for 5 h, and catalase groups are represented by the dashed line; $n = 4–6$. Influence of catalase inhibitor aminotriazole (ATZ) on EA-induced cytotoxicity is depicted in *C*. Cells were treated for 5 h, and ATZ is represented by dashed line; $n = 4$.

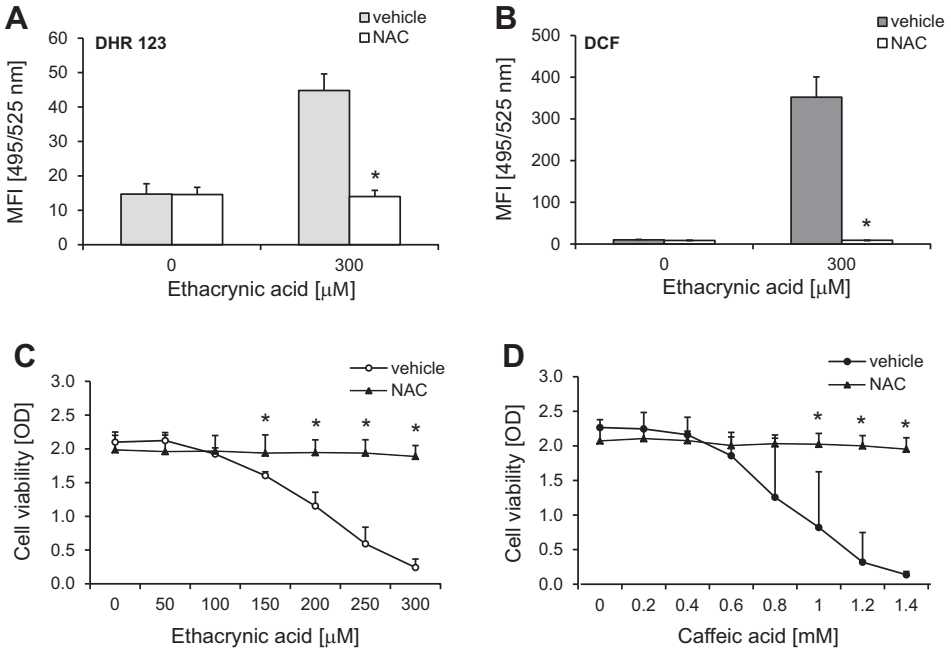

Fig. 7. Influence of *N*-acetyl cysteine (NAC) on EA-induced increase in fluorescence of redox-sensitive dyes DHR123 (*A*) and DCF (*B*) over 1 h; $n = 4$; $^*P < 0.05$ vs. vehicle control (in the absence of NAC). *C* and *D*: influence of NAC (▲) on EA-induced (○) (*C*) and CA-induced (●) (*D*) cell death, over 5 and 24 h, respectively, assessed by MTT assay; $n = 6$. $^*P < 0.05$ vs. vehicle control (in the absence of catalase or NAC).

GST inhibition has no influence on mitochondrial energetics. To investigate whether EA mediates cellular injury through oxidative stress affecting mitochondrial energetics, we determined ATP/ADP nucleotide ratios in extracts of cells exposed to EA, H_2O_2, or both treatments over 3 h and 5 h. In control cells, ATP levels were 27.6 ± 1.7 nmol/mg protein, and ADP levels were 2.1 ± 0.3 nmol/mg protein. ATP/ADP ratios were not affected by EA exposure alone, with ratios of 17 ± 2, 15 ± 1, and 20 ± 4 following exposure to 100 μM, 200 μM, and 300 μM respectively for 3 h. By contrast exposure of cells to H_2O_2, used as a positive control, significantly reduced ATP/ADP ratio from 12 ± 4 to 5 ± 3 after 5 h ($P < 0.05$). EA (100 μM) had no influence on H_2O_2-induced reduction in ATP/ADP ratio (5 ± 3 vs. 3 ± 2 nmol/mg protein, $P > 0.05$) (Fig. 8).

Changes in intracellular metabonomic profile. Metabonomics was employed to explore the impact of GST inhibitor EA and oxidative stress on global metabolic profile. ^{1}H-NMR spectra acquired from control, EA-, H_2O_2-, and H_2O_2 + EA-treated MLE cells. Spectral regions that could be assigned to specific metabolites, which showed visual evidence of variation in peak intensities, were subject to further analysis. Table 1 shows the fold change of assigned metabolites significantly affected by oxidative stress and EA. Changes in metabolite levels were enhanced after dual treatment with H_2O_2 and EA compared with treatment with EA or H_2O_2 alone. Metabolites with the most prominent changes in response to treatment with H_2O_2 and EA included glutamate (4.5-fold increase), threonine (4.2-fold increase), and tyramine (3.5-fold increase). Metabonomics also revealed a number of unassigned metabolites whose levels were altered by H_2O_2 and EA exposure.

Genetic manipulation of GST-π impacts on cell viability in control and stress conditions. To develop a cellular model of GSTM1-null and GSTP1 Ile^{105} polymorphisms, we investigated the impact of specific GST isoform knockdown by RNA interference. The efficiency of siRNA-mediated RNA knockdown was assessed by real-time PCR, 48 h following transfection. Cells transfected with GST-μ and -π siRNA showed 87 ± 4% and 90 ± 3% knockdown of RNA expression, respectively, with no significant effect of control scrambled siRNA (Fig. 9*A*). Protein expression of GST-μ and -π was evaluated by Western blotting 48 and 72 h after transfection. Whereas GST-π protein expression was abundant in A549 cell line and expressed in whole mouse lung, the expression of this protein was low in MLE cells (Fig. 9*C*), and therefore the influence of GST knockdown could not be monitored by Western blotting. However, protein bands indicate that GST-μ protein is absent in cells transfected with GST-μ siRNA at 48 and 72 h (Fig. 9*B*).

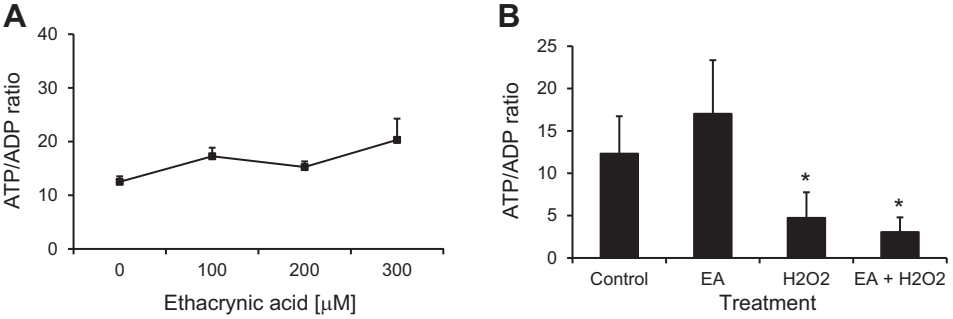

Fig. 8. Mitochondrial energetics was assessed by ATP/ADP ratio following increasing concentrations of EA over 3 h (*A*) and EA (100 μM) treatment and/or H_2O_2 (0.8 mM) over 5 h (*B*); $n = 3$; $^*P < 0.05$ vs. untreated control.

Table 1. *Fold change of selected metabolites significantly affected by EA and oxidative stress*

	EA	H_2O_2	H_2O_2 + EA	*P**
Threonine	2.0	2.4	4.2	0.016
Glutamate	1.6	2.1	4.5	0.016
Tyramine	1.5	1.9	3.5	0.019
Phenylalanine	1.5	2.0	3.2	0.022
Lactate	1.4	1.6	2.2	0.025
Pyruvate	1.4	1.1	1.5	0.022
Ox-glutathione	1.3	1.2	1.6	0.025
Alanine	1.2	1.2	1.4	0.025
Aspartate	1.1	1.2	1.6	0.034
Free choline	1.1	1.3	1.5	0.016
Glycerophosphocholine	1.3	1.0	1.8	0.024

Cells were exposed to either or both ethacrynic acid (100 μM) (EA) and/or oxidative stress (0.8 mM H_2O_2) over a 5-h period ($n = 3$). *Kruskal-Wallis test. Multiple comparisons were controlled for using the Benjamini-Hochberg procedure, with accepted false discovery rate of 0.05.

Oxidative stress was simulated by exposure of cells to H_2O_2 (3 h) or hypoxia (24 h) followed by reoxygenation for 6 h, and cell viability was assessed by MTT assay. GST-μ siRNA knockdown had no significant effect on cell viability alone or in response to H_2O_2 or HR. Interestingly GST-π knockdown resulted in a 16 ± 11% reduction in viability of control cells (Fig. 10*A*). Moreover, the viability of GST-π siRNA-transfected cells was significantly less than cells transfected with scrambled siRNA in the presence of 1 mM H_2O_2 (28 ± 10% vs. 49 ± 21%, $P < 0.05$) (Fig. 10*A*). As in previous experimental series, HR did not compromise MLE cell viability in control conditions (scrambled siRNA). However, lack of GST-π isoform resulted in a 20 ± 18% reduction in viability ($P < 0.05$) (Fig. 10*B*).

EA affects lung mechanics and permeability in the isolated perfused lung model. To begin to explore the physiological role of GST, we used an ex vivo IPL model and supplemented the perfusate with GST inhibitor EA. Pulmonary mechanics were monitored at 15-min intervals over the 2-h perfusion period. Physiological parameters remained stable and similar to control values for ~90 min of perfusion. However, EA supplementation resulted in a significant increase in plateau pressure (34%, $P < 0.05$) at 120 min (Fig. 11*A*). A similar increase in PIP was also observed (31%) at 120 min although this did not reach significance. We observed similar significant increases in pulmonary resistance (29 ± 19, $P < 0.05$) and elastance (33 ± 24%, $P < 0.05$) at 120 min in the presence of EA (Fig. 11, *B* and *C*).

Lung permeability was assessed via measurement of fluorescence-labeled albumin translocation from blood to alveolar space. BALF protein content was measured as an additional index of pulmonary edema. EA gave a threefold rise in the BALF:perfusate ratio, an index of epithelial barrier permeability (0.017 ± 0.009 vs. 0.052 ± 0.016, $P < 0.05$) (Fig. 11*D*), and a sixfold increase in BALF protein levels (0.7 ± 0.4 mg/ml vs. 4.3 ± 2.4 mg/ml, $P < 0.05$) (Fig. 11*E*).

DISCUSSION

There is increasing evidence from clinical literature that GST polymorphism and altered GST expression may impact on lung oxidative stress and outcomes of lung injury (7, 25, 32). Experimental data show that exogenous supplementation of recombinant GST enzymes impacts positively on oxidative events and inflammation (23), but the role of endogenous GSTs is less well known. The primary objective of this study was to explore the influence of attenuated endogenous GST activity in lung epithelial cells on cellular responses relevant to the setting of ischemia and reperfusion injury.

In the present study, we demonstrated that both pharmacological inhibition of endogenous GSTs and genetic knockdown of GST isoforms affected epithelial cell injury. First, two well recognized GST inhibitors, EA and CA (28, 29, 49), compromised cell viability in a concentration- and time-dependent manner. Concentrations inducing such cytotoxicity were com-

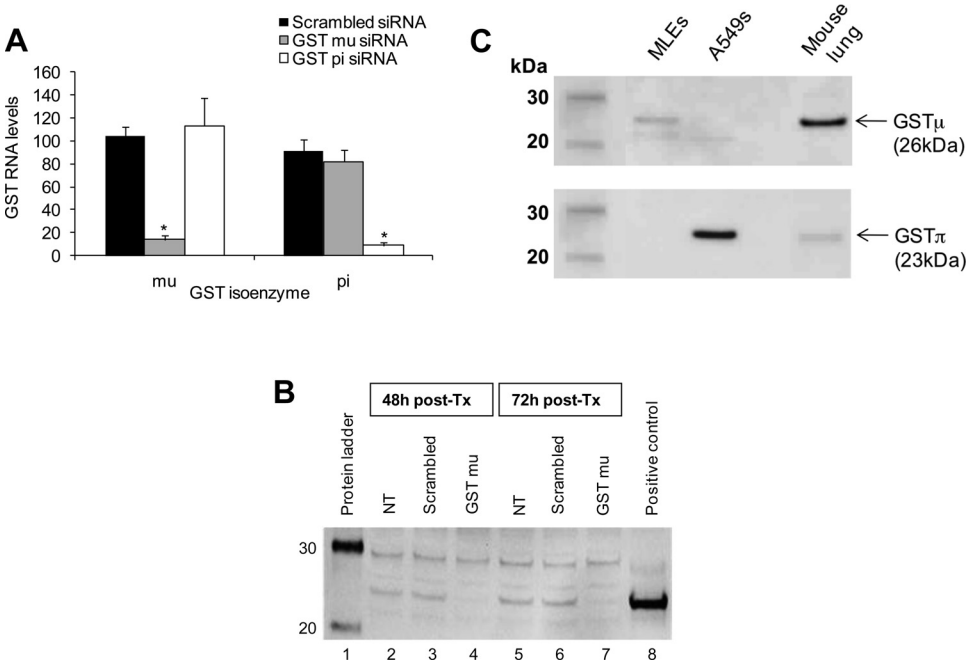

Fig. 9. Efficiency of GST-μ and -π siRNA and impact of GST isoform knockdown on MLE cells exposed to stress. *A*: GST-μ RNA expression measured by RT-PCR 48 h after cell transfection with scrambled, μ, and π siRNA; $n = 4$; *$P < 0.05$ vs. scrambled control. *B*: representative blot ($n = 3$) of GST-μ protein expression assessed by Western blotting 48 and 72 h after cells were nontransfected (NT), or transfected (Tx) with scrambled or GST-μ siRNA. *C*: Western blot analysis of GST-μ and -π protein expression in MLE and A549 cell lysates and whole mouse lung homogenate (as additional controls); $n = 2$.

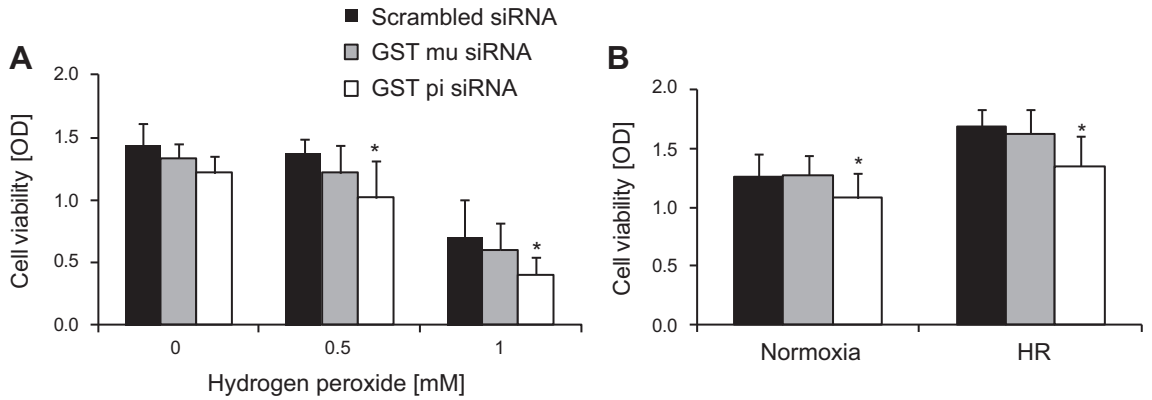

Fig. 10. Impact of GST isoform knockdown on MLE cells exposed to stress. The influence of GST-μ and -π attenuation on cellular response to chemical stress H_2O_2 at the indicated concentrations (over 3 h) is shown in *A* and to 24-h hypoxia and 6-h reoxygenation (HR) in *B*; $n = 4–6$; $^*P < 0.05$ vs. control cells transfected with scrambled siRNA.

parable to those inhibiting both pure GST and endogenous GST activity in MLE cell lysates. Although GST inhibitor-induced cell death was unexpected, such a response is not unprecedented, as similar observations were made in colon cancer cell lines and human leukemia cell lines (1, 37). In addition to causing cell injury themselves, subtoxic concentrations of EA and CA potentiated cytotoxicity induced by chemical stressors H_2O_2 and tBH. Although MLE cells tolerated long periods of hypoxia and subsequent reoxygenation, injury was unmasked in the presence of subtoxic concentrations of the GST inhibitor.

Genetic attenuation of GST-π following siRNA transfection resulted in a decrease in viability of nonstressed cells and rendered cells more susceptible to H_2O_2-induced injury and HR conditions. Although the magnitude of this response was less than those with pharmacological inhibition, this is remarkable considering the redundancy of intracellular GST enzymes.

Although our experiments may suggest a more specific involvement of GST-π, as knockdown of GST-μ did not have similar effects in MLE cells, these results should be interpreted with caution. First, we only targeted one GSTM gene, and other genes in this class could have compensated for such effect. Second, the abundance of GST-π in MLE cells was lower than GST-μ, and the effect of knockdown on cell viability, therefore, could have been related to protein abundance rather than specific activity. Nevertheless, our results suggest that endogenous GST-π could be important for normal homeostasis and viability of lung epithelial cells and in the intrinsic survival mechanisms of these cells under oxidative stress conditions and HR.

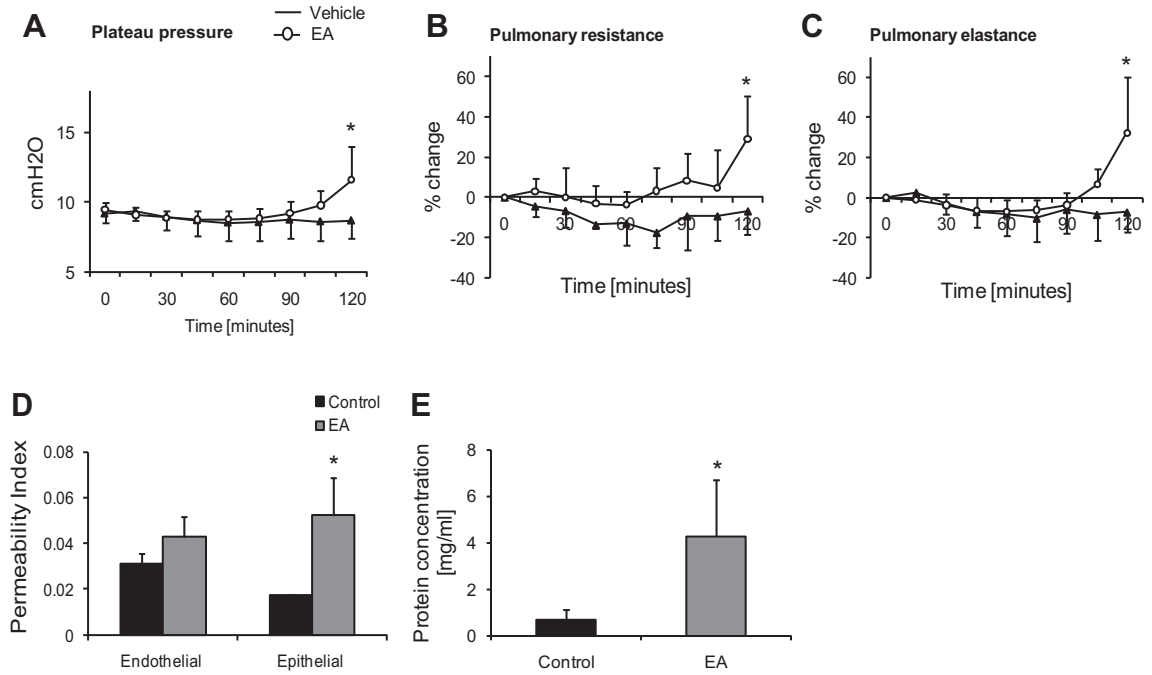

Fig. 11. Effect of EA-supplemented perfusion on pulmonary mechanics of mouse isolated perfused lung (over 120 min). Plateau pressure (*A*), pulmonary resistance (*B*), and pulmonary elastance (*C*) were all monitored at 15-min intervals in murine lungs perfused with control (▲) or EA-supplemented (100 μM) (○) perfusate. Influence of EA-supplemented perfusate on endothelial and epithelial barrier permeability (*D*) and bronchoalveolar lavage fluid protein content (*E*) are shown; $n = 3$; $^*P < 0.05$ vs. vehicle control.

Apoptosis of lung epithelial cells represents a potentially important mechanism contributing to the development of ALI in various settings. Two previous studies evaluated the role of apoptosis in EA-induced cell death in cancer cell lines and reported conflicting results (1, 37). By using flow cytometry, we observed a slight increase in the percentage of purely apoptotic cells following EA exposure; however, the majority of cells exhibited both annexin V and PI fluorescence, representing a late apoptotic/necrotic cell death. To further define the role of classical apoptotic events in EA-induced cell death, we investigated the involvement of caspases. EA-induced cell death was not affected by the caspase inhibitor, which in turn attenuated the response to another death stimulus (TNF in the presence of cycloheximide). Thus we concluded that EA-induced cytotoxicity is unlikely to be driven by a classical caspase-mediated apoptotic pathway. However, we cannot exclude the involvement of a caspase-independent apoptotic cascade, such as that mediated by apoptosis-inducing factor.

We have considered the possibility that the GST inhibitors increased intracellular oxidative stress, either through inhibition of GST leading to an accumulation of intracellular ROS or through direct activation of ROS-producing pathways. In previous studies, ROS accumulation has been implicated in EA-induced cell death (37); thus we investigated the influence of EA on various aspects of oxidative stress using complementary approaches. EA caused a significant increase in both DHR123 (2-fold) and DCF (30-fold) fluorescence in MLE cells. Although the exact mechanism responsible for the increased fluorescence and differential response with these probes remains unknown, the data provide evidence linking EA exposure to intracellular oxidative reactions. Although the limitation of DCF in detecting intracellular H_2O_2 is well established (15, 40), it is possible that EA-induced redox events may involve H_2O_2-triggered downstream oxidative reactions. Indeed, one previous study concluded that EA-induced cytotoxicity was mediated by H_2O_2 (37). In our experiments, however, H_2O_2 caused a dissimilar pattern of DCF/DHR123 increase compared with EA, and EA-induced cell injury was not prevented by PEG catalase or potentiated by endogenous catalase inhibition. A limitation of these experiments is that intracellular catalase activity was not measured. Furthermore, the application of DETC may not have been specific, as it affects all copper-containing molecules, not just CuZnSOD, and would not be expected to affect MnSOD. The DHR response indicates the possible involvement of reactive nitrogen species; however, L-NAME had no effect on EA responses. Therefore, we do not think that either H_2O_2 or nitric oxide plays a significant role in GST inhibitor-induced intracellular oxidative stress and cell death.

To further substantiate the role of redox events, we determined global intracellular redox state by measuring the prominent intracellular NAD^+/NADH redox couples. Cellular and mitochondrial redox homeostasis is intricately connected and regulated by several redox-sensitive couples, including glutathione/glutathione disulphide and NAD^+/NADH (2). We have shown the ability of EA to alter NAD^+/NADH ratio and a tendency to potentiate H_2O_2-induced redox changes. Furthermore, although low concentrations of EA did not cause protein carbonyl formation, EA significantly enhanced this reaction by H_2O_2. Taken together, these independent experiments suggest an association between EA-induced intracellular oxidative stress and cellular injury.

Interestingly, preincubation of cells with NAC prevented both EA- and CA-induced increase in ROS, as well as the resulting cell death. There may be several explanations for this phenomenon. First, NAC may interfere with the GST inhibitors themselves in the extracellular space. Although we cannot exclude such possibility with certainty, the fact that NAC inhibited the actions of two chemically distinct pharmacological GST inhibitors makes this scenario less likely. Moreover, Aizawa et al. (1) also concluded that the influence of NAC on EA-induced responses in their experiments was not related to direct interaction with EA (1). The second explanation is that NAC could augment intracellular antioxidant capacity by entering the cells and may help scavenge reactive species responsible for fluorescent dye oxidation and cellular injury. Third, NAC as a precursor of glutathione may augment or replenish depleted glutathione levels. Indeed, DCF fluorescence is modulated by intracellular glutathione, and glutathione is one of the major defense mechanisms guarding against intracellular oxidative stress. Finally, the effects of NAC may be unrelated to its antioxidant properties, as it is a very broad-spectrum reducing agent.

The effects of GST inhibitors on mitochondrial energetics and its influence on cell injury and necrosis were considered. As ATP/ADP ratio remained unchanged even by high concentrations of EA, we have concluded that mitochondrial dysfunction is an unlikely mediator of EA-induced cell death. Metabonomics profiling has provided a preliminary insight into the metabolic pathways affected in cells exposed to oxidant stress and/or GST inhibition. Initial multivariate analysis of acquired NMR spectral dataset separated treatment groups, suggesting that both oxidative stress and GST inhibition produce time- and treatment-specific changes in the global intracellular metabolome. Targeted spectral analysis identified specific changes in cellular metabolites in response to defined oxidative stress by H_2O_2, and many of these have close links to energy metabolism and cellular redox status and adaptation.

These metabolites have been previously reported to be associated with various ischemic, inflammatory, and oxidative conditions. For instance, glutamate acts as a neurotransmitter in various oxidative stress-related neurodegenerative conditions and has been linked to the development of lung injury in animal models of hyperoxia and sepsis (10, 30, 36). In addition, threonine levels increase in response to hypoxic injury (42), and elevated levels of tyramine have been reported following myocardial infarction, acute cystitis, and smoking (22, 27, 43). Further experimental work and bioinformatics analysis is required to determine the precise role of these metabolites in ischemia, oxidative stress, and inflammation.

It is clear that multiple oxidative stress-induced changes were modified by cotreatment with the GST inhibitor. By detecting differences in a number of unassigned peaks of the metabonomic spectra, our findings also reveal potentially novel metabolic signatures of oxidative stress and GST inhibition.

In addition to the in vitro studies, experiments were performed to explore the physiological consequences of GST inhibition. A mouse ex vivo lung perfusion model documented the direct pulmonary influence of EA supplementation. EA caused time-dependent changes in multiple aspects of physiology, in particular, increased respiratory elastance, resistance,

and pulmonary permeability. The experimental conditions did not affect perfusion pressure. These preliminary findings suggest that EA caused a degree of specific injury to lung compartments, most likely microvascular and epithelial permeability.

Despite the strengths of our investigation covering multiple aspects of endogenous GST-related oxidative stress, cellular energetics, and metabolism using complementary pharmacological and genetic approaches and expanding the in vitro findings to in vivo physiology, the study has limitations. First, our investigation focuses primarily on epithelial cells. We, however, realize that hypoxia/reperfusion injury requires damage to both epithelial and endothelial linings of the lung and the endothelium must be damaged for the increase in permeability and changes in lung mechanics to occur. There is published evidence regarding the roles for GST enzymes in modulating cellular responses of vascular endothelial cells and signaling pathways during oxidative stress (46, 48). Moreover, we show that the cytotoxic effect of EA is not restricted to epithelial cells, but the phenomenon is also observed in mouse endothelial cells. Our IPL data also demonstrate selective influence of EA on endothelial function as pulmonary artery pressure; hence pulmonary vascular resistance and vasoactivity was not altered, but microvascular permeability was increased. This phenomenon may be related to published evidence of GST regulating tight junction composition and organization (46).

Another limitation relates to using fluorescence markers of oxidative stress, which is liable to well-known limitations and potential artifacts (15, 40). We realize that fluorescent dyes only provide general information on the ability of the cells to oxidize the dyes and that the exact mechanism of these phenomena remains to be fully elucidated. However, we did not rely completely on these probes but assessed additional aspects of oxidative stress and multiple pharmacological strategies.

A further limitation is that most of the GST inhibition experiments used pharmacological tools that have the potential for off-target effects. Nevertheless, we obtained similar data using chemically distinct inhibitors and complemented the pharmacology with genetic approaches. Finally, our metabonomics and in vivo studies are preliminary in nature. Nevertheless, the metabolic profiling experiments have provided us with the first description of oxidative stress metabolome in lung epithelial cells. Furthermore, the physiological experiments clearly documented promising aspects of lung mechanics and permeability where endogenous GST may be essential. These may be helpful in the design of in vivo experiments for future studies, perhaps using GST conditional cell-specific knockout mice.

This work and other published literature should underpin more preclinical work with animal models toward new approaches to address lung injury in humans. The recognition that GST genes are consistently altered in various animal models of lung injury and are among the top genes that accurately predict development of primary graft failure in lung transplant donors (19) certainly points toward these promising directions. Our pilot genetic data may also highlight a role of specific GST gene polymorphism in the development of perioperative myocardial infarction (20), thus extending the paradigm beyond lung ischemia reperfusion injury.

In summary, we have demonstrated that alteration of GST activity disturbs the intracellular redox status, most likely through accumulation of secondary oxidative stress products. Furthermore, our findings suggest that GST inhibitors or specific attenuation of GST-π enhance H_2O_2-induced cell injury attributable to increased oxidative stress and subsequent metabolic derangements. The totality of evidence gathered in these studies demonstrates that GST activity is potentially involved in the survival of cultured lung epithelial cells under stress conditions. On the basis of our pilot physiological data, endogenous GST may play an important role in lung microvascular and epithelial regulation of permeability and lung mechanics and may have important clinical implications.

ACKNOWLEDGMENTS

We are thankful to Dr. Enrique Lara-Pezzi for guidance in siRNA and PCR technology.

GRANTS

M. Fletcher was supported by a PhD fellowship by the Westminster Medical School Research Trust.

DISCLOSURES

No conflicts of interest, financial or otherwise, are declared by the authors.

AUTHOR CONTRIBUTIONS

Author contributions: M.F. and N.M. conception and design of research; M.F., P.B., and K.W. performed experiments; M.F., P.B., K.W., and P.K. analyzed data; M.F., P.B., K.W., H.K., R.T.S., P.K., I.M.A., P.J.B., M.T., and N.M. interpreted results of experiments; M.F., P.B., and K.W. prepared figures; M.F. and N.M. drafted manuscript; M.F., P.B., K.W., H.K., R.T.S., P.K., I.M.A., P.J.B., M.T., and N.M. edited and revised manuscript; M.F., M.T., and N.M. approved final version of manuscript.

REFERENCES

1. **Aizawa S, Ookawa K, Kudo T, Asano J, Hayakari M, Tsuchida S.** Characterization of cell death induced by ethacrynic acid in a human colon cancer cell line DLD-1 and suppression by N-acetyl-L-cysteine. *Cancer Sci* 94: 886–893, 2003.
2. **Aon MA, Cortassa S, O'Rourke B.** Redox-optimized ROS balance: a unifying hypothesis. *Biochim Biophys Acta* 1797: 865–877, 2010.
3. **Backshall A, Alferez D, Teichert F, Wilson ID, Wilkinson RW, Goodlad RA, Keun HC.** Detection of metabolic alterations in non-tumor gastrointestinal tissue of the Apc(Min/+) mouse by (1)H MAS NMR spectroscopy. *J Proteome Res* 8: 1423–1430, 2009.
4. **Barker CE, Ali S, O'Boyle G, Kirby JA.** Transplantation and inflammation: implications for the modification of chemokine function. *Immunology* 143: 138–145, 2014.
5. **Brinkman NE, Haugland RA, Wymer LJ, Byappanahalli M, Whitman RL, Vesper SJ.** Evaluation of a rapid, quantitative real-time PCR method for enumeration of pathogenic Candida cells in water. *Appl Environ Microbiol* 69: 1775–1782, 2003.
6. **Burcham PC.** Modified protein carbonyl assay detects oxidised membrane proteins: A new tool for assessing drug- and chemically-induced oxidative cell injury. *J Pharmacol Toxicol Methods* 56: 18–22, 2007.
7. **Cantlay AM, Smith CA, Wallace WA, Yap PL, Lamb D, Harrison DJ.** Heterogeneous expression and polymorphic genotype of glutathione S-transferases in human lung. *Thorax* 49: 1010–1014, 1994.
8. **Christie JD, Aplenc R, DeAndrade J, Kawat S, Milstone A, Weinacker A, Zhou L, Mazzotta J, DeMissie E, Ely EW, Lung Tranplant Outcome Group.** Donor glutathione S-transferase genotype is associated with primary graft dysfunction following lung transplantation. *J Heart Lung Transplant* 24: S80, 2005.
9. **Cui Q, Lewis IA, Hegeman AD, Anderson ME, Li J, Schulte CF, Westler WM, Eghbalnia HR, Sussman MR, Markley JL.** Metabolite identification via the Madison Metabolomics Consortium Database. *Nat Biotechnol* 26: 162–164, 2008.
10. **da Cunha AA, Pauli V, Saciura VC, Pires MG, Constantino LC, de Souza B, Petronilho F, Rodrigues de Oliveira J, Ritter C, Romao PR, Boeck CR, Roesler R, Quevedo J, Dal-Pizzol F.** N-methyl-D-aspartate

glutamate receptor blockade attenuates lung injury associated with experimental sepsis. *Chest* 137: 297–302, 2010.
11. **Droge W.** Free radicals in the physiological control of cell function. *Physiol Rev* 82: 47–95, 2002.
12. **Felkin LE, Birks EJ, George R, Wong S, Khaghani A, Yacoub MH, Barton PJ.** A quantitative gene expression profile of matrix metalloproteinases (MMPS) and their inhibitors (TIMPS) in the myocardium of patients with deteriorating heart failure requiring left ventricular assist device support. *J Heart Lung Transplant* 25: 1413–1419, 2006.
13. **Felkin LE, Taegtmeyer AB, Barton PJ.** Real-time quantitative polymerase chain reaction in cardiac transplant research. *Methods Mol Biol* 333: 305–330, 2006.
14. **Hadjiliadis D, Lingaraju R, Mendez J, Pochettino A, Ahya VN, Sager JS, Kotloff RM, Christie JD.** Donor glutathione-s-transferase (GST) mu null genotype in lung transplant recipients is associated with increased rates of bronchiolitis obliterans syndrome (BOS) independent of acute rejection. *J Heart Lung Transplant* 26: S108, 2007.
15. **Halliwell B, Whiteman M.** Measuring reactive species and oxidative damage in vivo and in cell culture: how should you do it and what do the results mean? *Br J Pharmacol* 142: 231–255, 2004.
16. **Hayes JD, Flanagan JU, Jowsey IR.** Glutathione transferases. *Annu Rev Pharmacol Toxicol* 45: 51–88, 2005.
17. **Hayes JD, McLellan LI.** Glutathione and glutathione-dependent enzymes represent a co-ordinately regulated defence against oxidative stress. *Free Radic Res* 31: 273–300, 1999.
18. **Hayes JD, Pulford DJ.** The glutathione S-transferase supergene family: regulation of GST and the contribution of the isoenzymes to cancer chemoprotection and drug resistance. *Crit Rev Biochem Mol Biol* 30: 445–600, 1995.
19. **Hu P, Wang X, Haitsma JJ, Furmli S, Masoom H, Liu M, Imai Y, Slutsky AS, Beyene J, Greenwood CM, dos Santos C.** Microarray meta-analysis identifies acute lung injury biomarkers in donor lungs that predict development of primary graft failure in recipients. *PLoS One* 7: e45506, 2012.
20. **Kovacs V, Gasz B, Balatonyi B, Jaromi L, Kisfali P, Borsiczky B, Jancso G, Marczin N, Szabados S, Melegh B, Nasri A, Roth E.** Polymorphisms in glutathione S-transferase are risk factors for perioperative acute myocardial infarction after cardiac surgery: a preliminary study. *Mol Cell Biochem* 389: 79–84, 2014.
21. **Lavitrano M, Smolenski RT, Musumeci A, Maccherini M, Slominska E, Di Florio E, Bracco A, Mancini A, Stassi G, Patti M, Giovannoni R, Froio A, Simeone F, Forni M, Bacci ML, D'Alise G, Cozzi E, Otterbein LE, Yacoub MH, Bach FH, Calise F.** Carbon monoxide improves cardiac energetics and safeguards the heart during reperfusion after cardiopulmonary bypass in pigs. *FASEB J* 18: 1093–1095, 2004.
22. **Liu YT, Jia HM, Chang X, Cheng WH, Zhao X, Ding G, Zhang HW, Cai DY, Zou ZM.** Metabolic pathways involved in Xin-Ke-Shu protecting against myocardial infarction in rats using ultra high-performance liquid chromatography coupled with quadrupole time-of-flight mass spectrometry. *J Pharm Biomed Anal* 90: 35–44, 2014.
23. **Luo L, Wang Y, Feng Q, Zhang H, Xue B, Shen J, Ye Y, Han X, Ma H, Xu J, Chen D, Yin Z.** Recombinant protein glutathione S-transferases P1 attenuates inflammation in mice. *Mol Immunol* 46: 848–857, 2009.
24. **Miyanishi K, Takayama T, Ohi M, Hayashi T, Nobuoka A, Nakajima T, Takimoto R, Kogawa K, Kato J, Sakamaki S, Niitsu Y.** Glutathione S-transferase-pi overexpression is closely associated with K-ras mutation during human colon carcinogenesis. *Gastroenterology* 121: 865–874, 2001.
25. **Moradi M, Mojtahedzadeh M, Mandegari A, Soltan-Sharifi MS, Najafi A, Khajavi MR, Hajibabayee M, Ghahremani MH.** The role of glutathione-S-transferase polymorphisms on clinical outcome of ALI/ARDS patient treated with N-acetylcysteine. *Respir Med* 103: 434–441, 2009.
26. **Mosmann T.** Rapid colorimetric assay for cellular growth and survival: application to proliferation and cytotoxicity assays. *J Immunol Methods* 65: 55–63, 1983.
27. **Mueller DC, Piller M, Niessner R, Scherer M, Scherer G.** Untargeted metabolomic profiling in saliva of smokers and nonsmokers by a validated GC-TOF-MS method. *J Proteome Res* 13: 1602–1613, 2014.
28. **Ploemen JH, van Ommen B, Bogaards JJ, van Bladeren PJ.** Ethacrynic acid and its glutathione conjugate as inhibitors of glutathione S-transferases. *Xenobiotica* 23: 913–923, 1993.
29. **Ploemen JH, van Ommen B, de Haan A, Schefferlie JG, van Bladeren PJ.** In vitro and in vivo reversible and irreversible inhibition of rat glutathione S-transferase isoenzymes by caffeic acid and its 2-S-glutathionyl conjugate. *Food Chem Toxicol* 31: 475–482, 1993.
30. **Said SI, Berisha HI, Pakbaz H.** Excitotoxicity in the lung: N-methyl-D-aspartate-induced, nitric oxide-dependent, pulmonary edema is attenuated by vasoactive intestinal peptide and by inhibitors of poly(ADP-ribose) polymerase. *Proc Natl Acad Sci USA* 93: 4688–4692, 1996.
31. **Smolenski RT, Lachno DR, Ledingham SJ, Yacoub MH.** Determination of sixteen nucleotides, nucleosides and bases using high-performance liquid chromatography and its application to the study of purine metabolism in hearts for transplantation. *J Chromatogr* 527: 414–420, 1990.
32. **Strange RC, Fryer AA.** The glutathione S-transferases: influence of polymorphism on cancer susceptibility. *IARC Sci Publ* 148: 231–249, 1999.
33. **Uchida K, Kanematsu M, Sakai K, Matsuda T, Hattori N, Mizuno Y, Suzuki D, Miyata T, Noguchi N, Niki E, Osawa T.** Protein-bound acrolein: potential markers for oxidative stress. *Proc Natl Acad Sci USA* 95: 4882–4887, 1998.
34. **von Bethmann AN, Brasch F, Nusing R, Vogt K, Volk HD, Muller KM, Wendel A, Uhlig S.** Hyperventilation induces release of cytokines from perfused mouse lung. *Am J Respir Crit Care Med* 157: 263–272, 1998.
35. **Wakabayashi K, Wilson MR, Tatham KC, O'Dea KP, Takata M.** Volutrauma, but not atelectrauma, induces systemic cytokine production by lung-marginated monocytes. *Crit Care Med* 42: e49–e57, 2014.
36. **Wang M, Luo Z, Liu S, Li L, Deng X, Huang F, Shang L, Jian C, Yue S.** Glutamate mediates hyperoxia-induced newborn rat lung injury through N-methyl-D-aspartate receptors. *Am J Respir Cell Mol Biol* 40: 260–267, 2009.
37. **Wang R, Li C, Song D, Zhao G, Zhao L, Jing Y.** Ethacrynic acid butyl-ester induces apoptosis in leukemia cells through a hydrogen peroxide mediated pathway independent of glutathione S-transferase P1-1 inhibition. *Cancer Res* 67: 7856–7864, 2007.
38. **Wang WZ, Fang XH, Stephenson LL, Khiabani KT, Zamboni WA.** Ischemia/reperfusion-induced necrosis and apoptosis in the cells isolated from rat skeletal muscle. *J Orthop Res* 26: 351–356, 2008.
39. **Wang X, Pavelic ZP, Li Y, Gleich L, Gartside PS, Pavelic L, Gluckman JL, Stambrook PJ.** Overexpression and amplification of glutathione S-transferase pi gene in head and neck squamous cell carcinomas. *Clin Cancer Res* 3: 111–114, 1997.
40. **Wardman P.** Fluorescent and luminescent probes for measurement of oxidative and nitrosative species in cells and tissues: progress, pitfalls, and prospects. *Free Radic Biol Med* 43: 995–1022, 2007.
41. **Ware LB, Matthay MA.** The acute respiratory distress syndrome. *N Engl J Med* 342: 1334–1349, 2000.
42. **Weljie AM, Bondareva A, Zang P, Jirik FR.** (1) H NMR metabolomics identification of markers of hypoxia-induced metabolic shifts in a breast cancer model system. *J Biomol NMR* 49: 185–193, 2011.
43. **Wen H, Lee T, You S, Park SH, Song H, Eilber KS, Anger JT, Freeman MR, Park S, Kim J.** Urinary metabolite profiling combined with computational analysis predicts interstitial cystitis-associated candidate biomarkers. *J Proteome Res* 14: 541–548, 2015.
44. **Wilson MR, Choudhury S, Goddard ME, O'Dea KP, Nicholson AG, Takata M.** High tidal volume upregulates intrapulmonary cytokines in an in vivo mouse model of ventilator-induced lung injury. *J Appl Physiol* 95: 1385–1393, 2003.
45. **Wilson MR, Goddard ME, O'Dea KP, Choudhury S, Takata M.** Differential roles of p55 and p75 tumor necrosis factor receptors on stretch-induced pulmonary edema in mice. *Am J Physiol Lung Cell Mol Physiol* 293: L60–L68, 2007.
46. **Xu Y, Gong B, Yang Y, Awasthi YC, Woods M, Boor PJ.** Glutathione-S-transferase protects against oxidative injury of endothelial cell tight junctions. *Endothelium* 14: 333–343, 2007.
47. **Yang MS, Yu LC, Gupta RC.** Analysis of changes in energy and redox states in HepG2 hepatoma and C6 glioma cells upon exposure to cadmium. *Toxicology* 201: 105–113, 2004.
48. **Yang Y, Yang Y, Trent MB, He N, Lick SD, Zimniak P, Awasthi YC, Boor PJ.** Glutathione-S-transferase A4-4 modulates oxidative stress in endothelium: possible role in human atherosclerosis. *Atherosclerosis* 173: 211–221, 2004.
49. **Zhao G, Yu T, Wang R, Wang X, Jing Y.** Synthesis and structure-activity relationship of ethacrynic acid analogues on glutathione-s-transferase P1-1 activity inhibition. *Bioorg Med Chem* 13: 4056–4062, 2005.